Table S1. Genes potentially involved in indole-3-acetic acid (IAA) biosynthesis in strain *Methylobacterium cistanchei* JK268^T based on KEGG orthology (KO) annotations. Representative locus tags are shown for each gene/module. These genomic features are consistent with the observed IAA-producing phenotype (Fig.S4), although the exact biosynthetic route requires further verification.

Pathway module	Gene(s)/system	KO (KEGG)	Representative locus tag(s)	Putative role / rationale (revised)
Tryptophan biosynthesis	*trpE, trpG, trpD, trpF, trpC, trpB, trpA*	K01657; K01658; K00766; K01817; K01609; K01696; K01695	JK268_trp_cluster	Supports de novo tryptophan biosynthesis, providing precursor supply for Trp-dependent IAA formation.
Aromatic aminotransferase	*tyrB*	K00832	JK268_GM002938	Putative aminotransferase converting tryptophan to indole-3-pyruvate – like intermediates (non pathway-specific).
Monoamine oxidase	*MAO*	K00274	JK268_GM001028; JK268_GM003240; JK268_GM004535	Converts tryptamine to indole-3-acetaldehyde, suggesting involvement in the TAM pathway of IAA biosynthesis.
Aldehyde dehydrogenase	*ALDH*	K00128	JK268_GM001453; JK268_GM000159	Catalyzes oxidation of indole-3-acetaldehyde to IAA, representing the final step in IAA formation.
Amidase	*amiE*	K01426	JK268_GM001712	General amide hydrolysis enzyme; insufficient evidence for a complete *IAM* pathway in absence of *iaaM/iaaH.*
Threonine dehydratase	*tdcB*	K01754	JK268_GM000924; JK268_GM004920; JK268_GM005953	Associated with amino acid metabolism; may contribute indirectly to tryptophan-derived metabolic flux.
Deaminase	*tdcF*	K09022	JK268_GM001861; JK268_GM005566	Involved in amino acid catabolism; may support precursor supply for IAA biosynthesis.

Table S2. Genomic features potentially underlying the antagonistic activity of strain *Methylobacterium cistanchei* JK268T identified by genome mining. These genomic features are consistent with the observed antagonistic activity phenotype (Fig.S5), although the exact biosynthetic route requires further verification.

Category	Gene(s)/system/ BGC	KO (KEGG)	Representative locus tag (s)	Potential contribution to antagonistic activity
Siderophore-mediated antagonism	NRPS (*SidA/IucD/PvdA/ MbtH*)	K01657; K01658; K00766; K01817; K01609; K01696; K01695	JK268_GM004841 (*SidA/IucD/PvdA*) JK268_GM004843(*MbtH*)	The presence of siderophore biosynthesis, transport and uptake-related genes suggests potential iron-chelating ability, which may contribute to competition with *Fusarium acuminatum* through iron limitation
Bioactive polyketide biosynthesis	T1PKS	K00832	JK268_GM005181 JK268_GM005196 JK268_GM005197 JK268_GM005200	Type 1 PKS-associated enzymes may participate in the biosynthesis and modification of bioactive polyketides with potential antifungal activity
Non-ribosomal peptide biosynthesis	NRPS (*Pls/PosA*)	K00274	JK268_GM005287	Indicates additional NRPS-related secondary metabolite biosynthetic capacity and potential production of unexplored peptide-derived metabolites
Secondary metabolite regulation and microbial interaction	ALH(*luxI/luxR*)	K01426	JK268_GM002403(*luxR*) JK268_GM002408(*luxr*)	AHL-mediated signaling may regulate microbial communication, secondary metabolism and competitive interactions
Antibacterial peptide production	Bacteriocin	K00128	JK268_GM000007 JK268_GM000008 JK268_GM000009	Suggests the potential production or modification of antimicrobial peptide-like compounds involved in microbial competition
Oxidative stress resistance	ROS(*katG/katE/sod*)	K01754	JK268_GM003494 (*katG*) JK268_GM004924 (*katE*) JK268_GM000695 (*sod1*) JK268_GM002727 (*sod2*)	ROS detoxification systems may enhance bacterial survival during antagonistic interactions and improve ecological competitiveness

Fig. S1. Neighbour-joining phylogenetic tree based on a comparison of the 16S rRNA gene sequences, showing the positions of strain JK268^T and its closest relatives. GenBank accession numbers are shown in parentheses. Evolutionary distances were calculated using the Tamura-Nei model. Bar, 0.01 nucleotide substitutions per site. Bootstrap values (>70%) based on 1000 replications are indicated at the nodes.

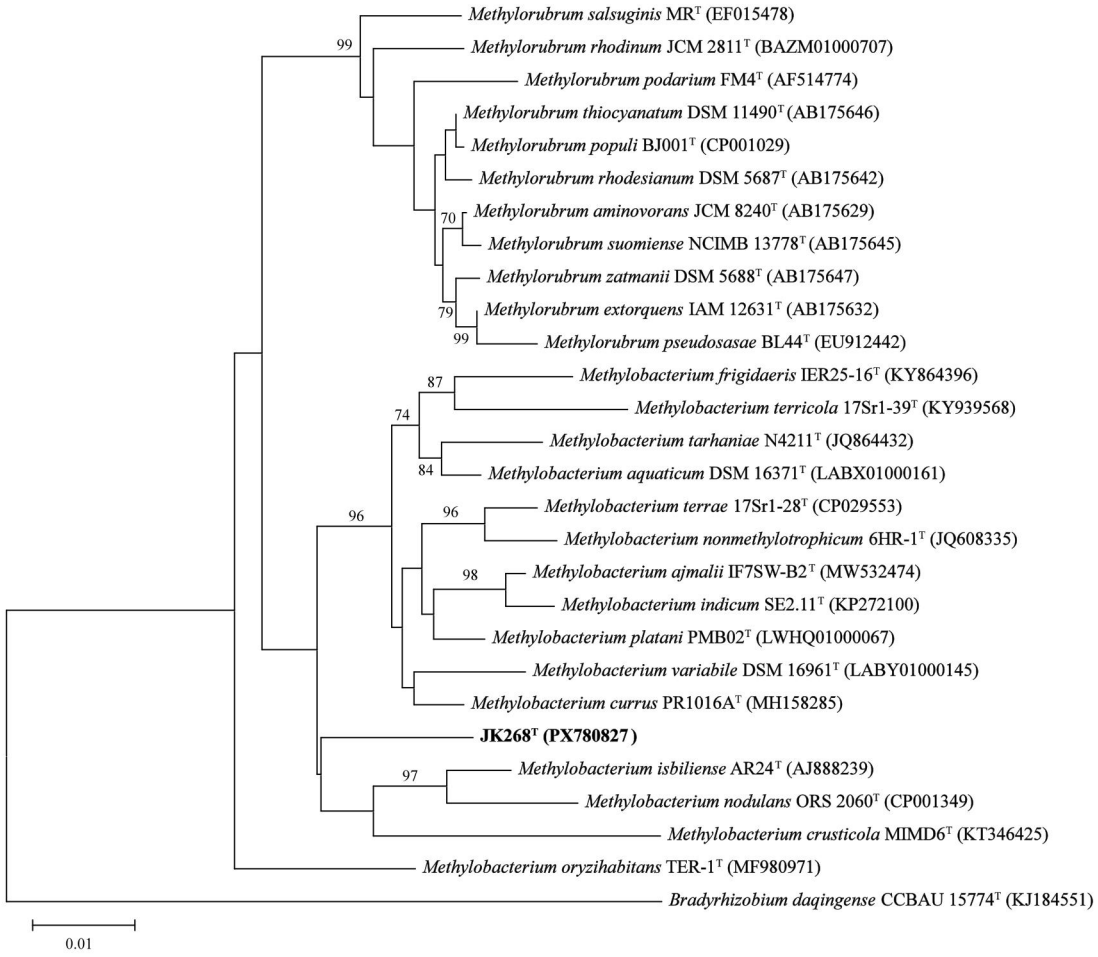


Fig. S2. Maximum-parsimony phylogenetic tree based on 16S rRNA gene sequences showing the position of strain JK268^{T} and its closest relatives. GenBank accession numbers are shown in parentheses. The tree was inferred using the subtree-pruning-regrafting algorithm with 10 random addition sequences. Bar, 5 nucleotide substitutions per site. Bootstrap values (>70%) based on 1000 replications are shown at the nodes.

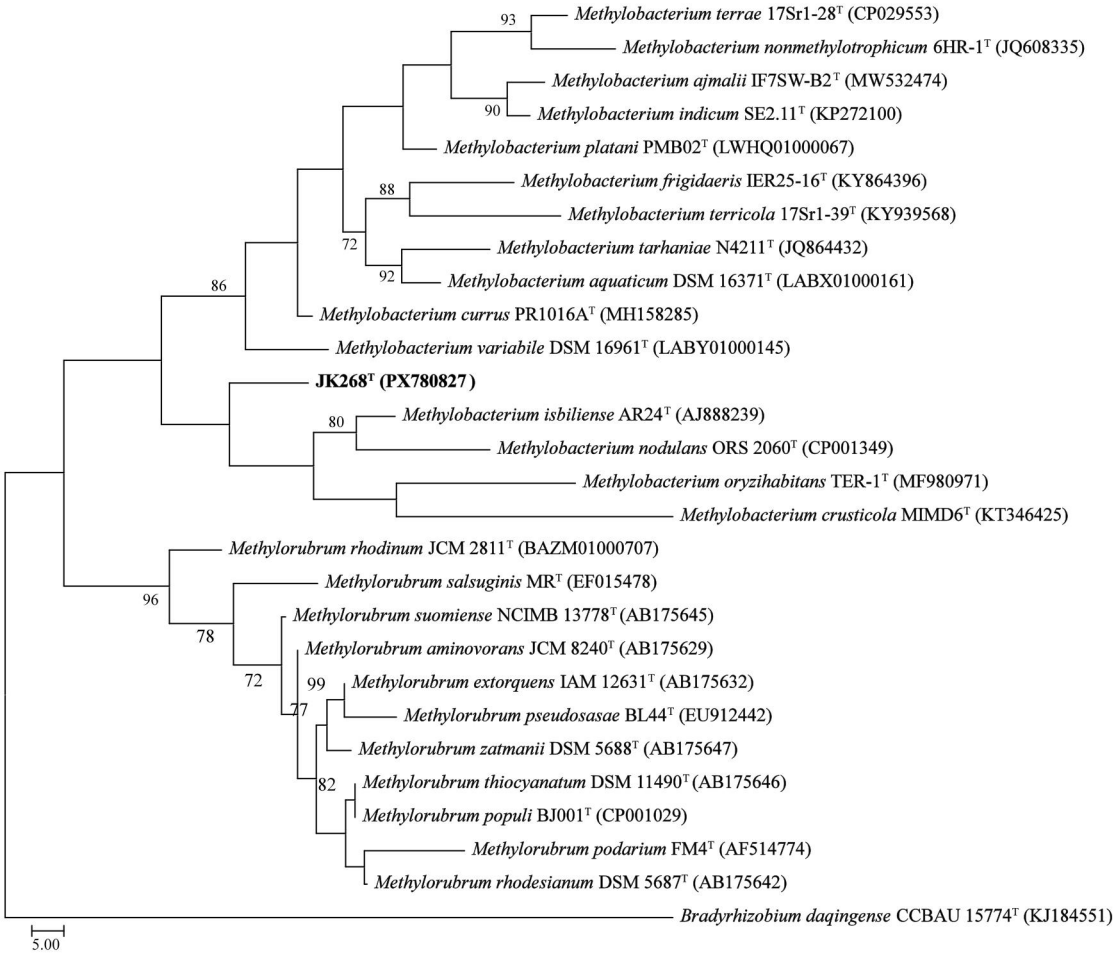


Fig. S3. Whole-genome phylogenomic tree showing the relationships between strain JK268^{T} and its closest related type species. The tree was inferred using EasyCGTree (v4.2) based on a concatenated supermatrix of 120 bacterial single-copy marker proteins (bac 120), followed by inference with FastTree. Branch lengths are scaled in terms of substitutions per site. Numbers at nodes indicate FastTree local support values (shown as percentages); values <70% are not shown. Genome accession numbers are shown in parentheses. *Azotobacter vinelandii* IAM 15004^{T} was used as the outgroup to root the tree.

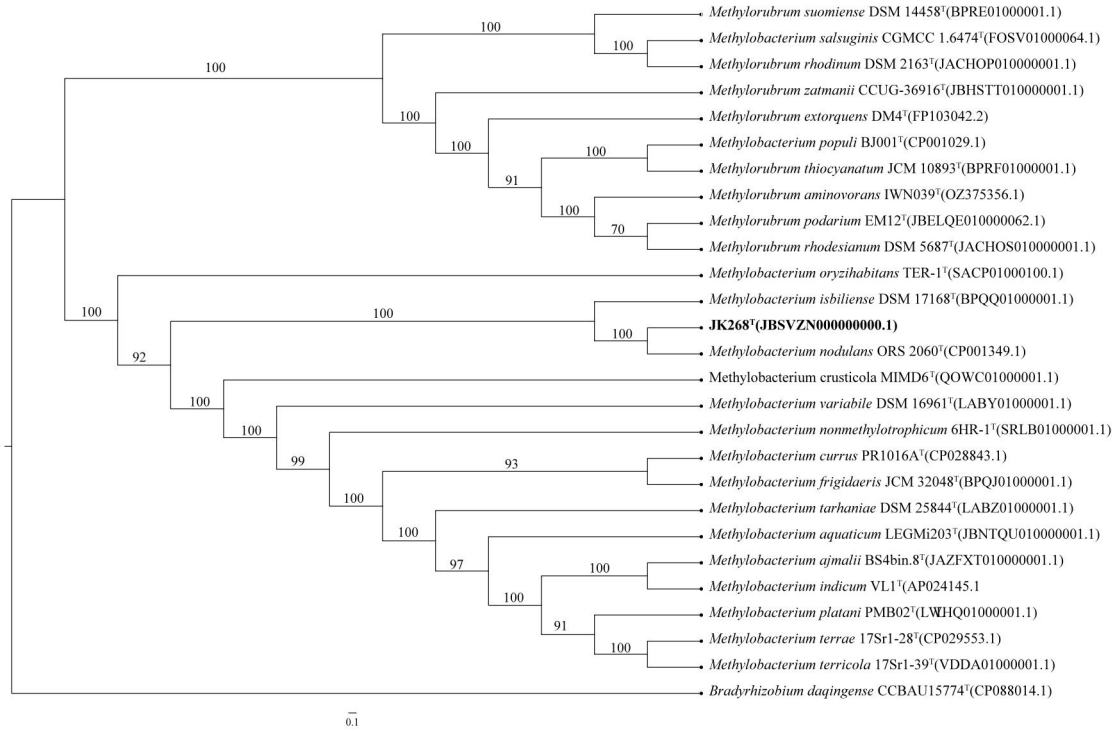


Fig. S4. Indole-3-acetic acid (IAA) production by strain JK268^T

(A) Representative colour development in the Salkowski reaction after incubation in the dark for 30 min.

(B) Standard curve for IAA quantification using the Salkowski colorimetric assay (ΔOD_{530}, uninoculated medium control subtracted).

(C) IAA production by strain JK268^T compared with an uninoculated LB control. Strain JK268^T was cultured in LB broth supplemented with L-tryptophan (100 mg L^{-1}) at 37 °C for 3 d. Cultures were centrifuged at 6000 rpm for 15 min at 4 °C, and the supernatant was mixed with Salkowski reagent at a 1:1 (v/v) ratio (100 µL each) and incubated in the dark for 30 min prior to measurement at 530 nm. ΔOD_{530} values were blank-subtracted using an uninoculated LB medium control. Data are presented as mean ± SD (n = 3). Statistical significance was assessed using a two-tailed unpaired Student's t test ($P < 0.0001$).

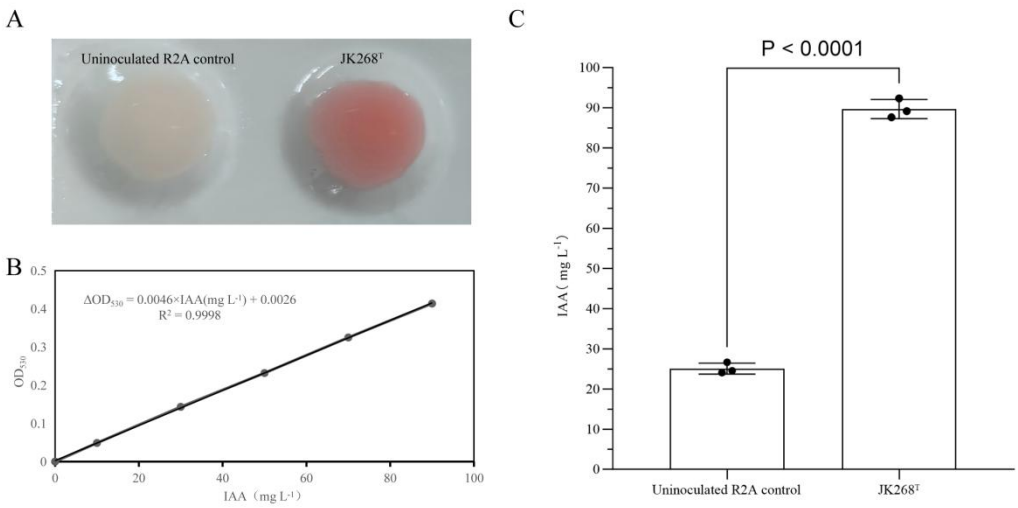


Fig. S5 In vitro antagonistic activity of strain JK66^{T} against *Fusarium acuminatum*.

(a) *F. acuminatum* grown on PDA as the control.

(b) Confrontation assay on PDA showing *F. acuminatum* co-cultured with bacterial isolates. The fungal plug was placed at the plate center, and bacterial inocula were point-inoculated with sterile toothpicks at a distance of 1.5 cm from the fungal inoculation point. Plates were incubated at 28 °C for 72 h. Compared with the control, strain JK268^{T} reduced radial growth of *F. acuminatum* toward the bacterial colony, indicating inhibitory (antagonistic) activity under the tested conditions.

(c) Antifungal activity of the cell-free fermentation broth of strain JK268^{T} against *F. acuminatum*. PDA plates supplemented with 20% (v/v) fermentation broth showed reduced fungal growth compared with the untreated control, with an inhibition rate of 47.76%, indicating that extracellular metabolites produced by strain JK268^{T} contributed to the antifungal activity.

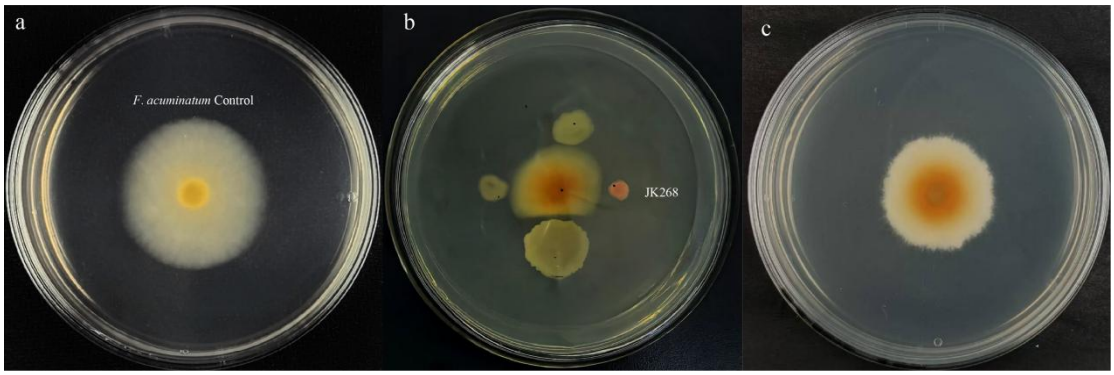


Fig. S6. Transmission electron micrograph of strain JK268^{T} showing rod-shaped cells with flagella. Bar, 500 nm.

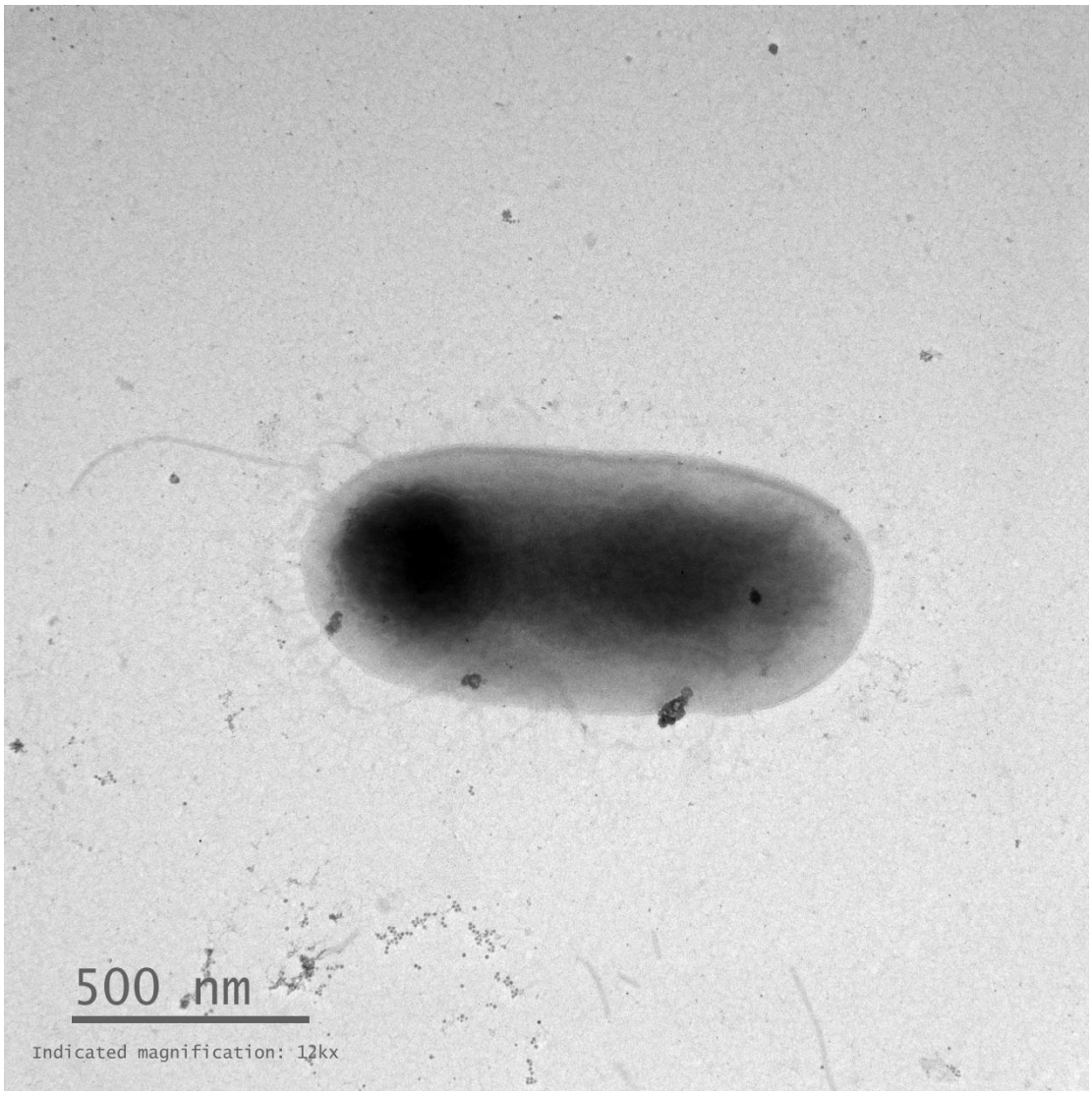


Fig. S7. Two-dimensional thin-layer chromatography (2D-TLC) of the polar lipids of strain JK268^T. The polar lipids detected were diphosphatidylglycerol (DPG);, phosphatidylglycerol (PG), phosphatidylethanolamine (PE), phosphatidylcholine (PC). Plates were stained with (a) molybdatophosphoric acid, (b) ninhydrin, (c) molybdatophosphoric acid, and (d) *α*-naphthol.

